Chapter Six: A Study of Secondary Organic Aerosols Formed From the Photooxidation of Anthropogenic and Biogenic Precursors in A Reaction Chamber

6.1 Introduction

In-situ investigation of key physical and chemical processes during secondary organic aerosol (SOA) formation in the atmosphere is complicated by the vast number of species involved and their generally low concentrations. Hence reaction chambers are often used to study these processes. A reaction chamber is a large confined volume in which sunlight or simulated sunlight is used to irradiate mixtures of atmospheric trace gases (hydrocarbons, nitrogen oxides, sulphur dioxide, etc.) in purified air. Experiments are generally carried out in a "batch" configuration, where reactants are mixed and the reaction is started without introducing any more new air or reactants, and the composition of the chamber is monitored in real-time or through sampling followed by off-line analysis. Reactions may also be carried out in the dark for some chemical systems. Reaction chambers can be used to produce controlled atmospheres to investigate a range of physical phenomena from the formation of gas-phase reaction products to the partitioning of semi-volatile compounds between the gas and particle phase. Such experiments can be useful in understanding the chemical and physical parameters that control the formation of secondary organic aerosols.

A number of reaction chamber studies have investigated gas-particle partitioning of products of photochemical reactions involving anthropogenic as well as biogenic precursors. Much of the efforts have been made to quantify the aerosol formation potential (aerosol yield) of small aromatic and natural hydrocarbon compounds both in the absence and presence of seed aerosol particles [*Odum et al., 1996; Odum et al., 1997; Griffin et al., 1999; Kleindienst et al., 1999; Aschmann et al., 2002*]. Other studies have attempted to identify the molecular composition of the oxidation products of anthropogenic and biogenic precursors, mainly aromatic and monoterpene compounds, and have offered detailed molecular mechanisms for the formation of various chemical species [*Forstner et al., 1997; Glasius et al., 2000; Jang and Kamens, 2001; Larsen et al., 2001; Griffin et al., 2002; Jaoui and Kamens, 2003; Kleindienst et al., 2004*]. In most of the studies, aerosol particles were collected on filters, extracted

with solvents and then analysed off-line, using gas chromatography-mass spectrometry (GC-MS). Only 10 – 30% of the mass collected and extracted could be identified on a molecular level [*Forstner et al., 1997; Cocker et al., 2001*].

Recent studies have reported that polymers and oligomers compose significant fractions of SOA formed from the photooxidation of aromatic and biogenic compounds. *Kalberer et al.*, [*2004*] found that about 50% of the SOA mass, formed from the photooxidation of 1,3,5-trimethylbenzene in a reaction chamber, consists of polymers with molecular masses of up to 1000 Daltons. Moreover, the formation of oligomeric molecules has been reported as an important step in the SOA production by the reaction of α-pinene and ozone in the presence of acid seed aerosol [*Tolocka et al., 2004a*]. The study reported in this chapter follows on from *Kalberer et al.*, [*2004*] and employs the Aerodyne aerosol mass spectrometer (AMS) to provide on-line measurements of the mass spectral signatures and mass size distributions of the oxidation products resulting from irradiating 1,3,5-trimethylbenzene (1,3,5-TMB, anthropogenic precursor) and α-pinene (biogenic precursor), separately, in the presence of nitrogen oxide, nitrogen dioxide and propene in a reaction chamber.

Unlike most other studies, the objective is not to provide detailed chemical speciation of the photooxidation products of both precursors. This is due to the fact that the AMS does not utilise any means of chemical separation prior to the vaporisation and ionisation of the particles (see chapter 3, section 3.5) [*Jayne et al., 2000; Jimenez et al., 2003b*]. Rather, this chapter aims to study the change in the highly time resolved chemical signatures of the products from each precursor as a function of irradiation time, and to compare the chemical signatures of the SOA formed from these two precursors. In addition, the study attempts to investigate the extent of oxidation and polymerisation of the aerosol-phase reaction products. Finally, the implications of the photooxidation reactions carried out in this study on atmospheric measurements are discussed by comparing the mass spectral signatures of the products of both precursors to ambient mass spectra of organic aerosols measured in various environments. Aerosol particles have been directly sampled from the reaction chamber into the AMS, avoiding

any artefacts (e.g. evaporation, adsorption, filter contamination) usually associated with the off-line analysis methods.

6.2 Experimental methodology

6.2.1 Reaction chamber

Experiments were carried out in the indoor reaction chamber at Paul Scherrer Institute (PSI), Switzerland, during a two-week period in February 2004. The PSI reaction chamber is a 27 m^3 transparent *Teflon®* bag suspended in a temperature-controlled housing. The radiation was generated by four xenon arc lamps (4 kW each) selected to simulate the solar light spectrum and natural photochemistry. The construction of the facility and its operation are described in more detail elsewhere [*Paulsen et al., 2004*].

6.2.2 Instrumentation

The Aerodyne aerosol mass spectrometer (AMS) was used to provide on-line quantitative measurements of the chemical composition and mass size distributions of the non-refractory fraction of aerosol particles at a temporal resolution of two min. Total particle number concentration (diameter D_p > 3nm) was monitored with a condensation particle counter (CPC, TSI model 3025). A scanning mobility particle sizer (SMPS) consisting of a differential mobility analyser (DMA, TSI model 3071) and a condensation particle counter (CPC, TSI model 3022) was used to measure particle size distributions from 7 to 316 nm. A volatility tandem differential mobility analyser (VTDMA) was used to measure the volatile fraction of size-selected particles as described in a previous publication [*Kalberer et al., 2004*]. The following gas phase components were also measured: CO (AeroLaser AL5002, Country), NO and NO_x (Make, ML 9841A and Thermo Environmental Instruments 42C retrofitted with a photolytic converter, Country), O_3 (UV-photometer: Environics S300, Country), the precursor hydrocarbons and their oxidation products with a proton transfer reaction - mass spectrometer (PTR-MS, Ionicon, Country).

6.2.3 Experimental conditions

Three experiments were carried out in the reaction chamber using each of the precursors, two of which were at ‘high’ concentration and one was at ‘low’

concentration. Table 6.1 summarises the initial conditions for each experiment. The 'high' concentration levels were chosen to provide good signal statistics for the AMS, whereas the low concentration levels were chosen to be as close as possible to atmospherically relevant concentrations, while taking into account instrument detection limits. The chamber was purged with purified air and water vapour for at least 24 hours before each experiment. Primary gas components including precursor, nitrogen oxides, purified air and water vapour were introduced into the chamber where they allowed to mix for approximately 45 min before the lights were turned on. Precursors were irradiated in the presence of NO_x and propene at nominally 50% relative humidity for durations between 8 and 20 hours. NO_x were added primarily to facilitate the basic photochemical cycle involving O_3 [*Seinfeld and Pandis, 1998; Griffin et al., 1999; Finlayson-Pitts and Pitts, 2000*], while propene was used as a photochemical initiator to provide OH radicals at sufficient levels for the inception of the experiment [*Odum et al., 1996; Forstner et al., 1997; Griffin et al., 1999; Kleindienst et al., 1999*].

Experiment	Precursor	Concentration (ppbv)	NO (ppbv)	NO_2 (ppbv)	Propene (ppbv)
1	1,3,5-TMB	35	11	8	300
2	1,3,5-TMB	620	150	150	300
3	1,3,5-TMB	620	150	150	300
4	α-Pinene	160	94	77	300
5	α-Pinene	30	55	68	300
6	α-Pinene	160	59	67	300

Table 6.1: Summary of conditions at the start of each experiment

6.3 Overview of secondary organic aerosol (SOA) formation

The non-volatile and semivolatile products from a photochemical reaction of an organic precursor accumulate with ongoing irradiation and when their gas phase saturation concentrations are exceeded, they begin to condense on pre-existing particles or, in the absence of seed aerosol particles, form new particles by homogeneous nucleation. The amount of a product that partitions into the particle phase is the quantity in excess of its gas phase saturation concentration [*Odum et al., 1996*]. However, *Pankow* [*1994b; 1994a*] has suggested that, once organics have begun to condense and an organic layer has formed on the particles, even products whose gas phase concentrations are below their saturation concentrations will partition a portion of their mass into this condensed

organic phase. Nucleation, condensation and subsequent adsorption and absorption of oxidation products lead to particles that are 100% organic in composition. The quantity of aerosol produced in this case, estimated from the final aerosol volume after accounting for wall losses, provides a measure of the SOA formation potential in a clean environment.

A representative time profile of the particles evolution during a 'high' concentration 1,3,5-TMB experiment (experiment number 3, Table 1) is illustrated in Figure 6.1. The total particle number concentration (p cm^{-3}) counted by the CPC, is shown in the top panel, the total mass loading (μg m^{-3}) measured by the AMS is presented in the middle panel and the bottom panel shows particle mass size distribution measured as a function of its vacuum aerodynamic diameter. In general, the shapes of the time dependent number concentration and mass loading curves as well as particle mass size distributions were similar for all experiments, though their absolute values depended on the organic precursor and its initial concentration.

Each experiment began with a nucleation event marked by the increasing number concentration of particles, which then grew by condensation and coagulation as reflected in the increasing particle diameters. CPC data for the experiment in Figure 6.1 show that particles grew to detectable sizes (> 3 nm) about half an hour after the lights were turned on and their number concentration increased rapidly to peak at about 35000 cm^{-3} within another 40 min. During experiment number 3, The total mass loading of particles increased with ongoing particle formation and condensational growth and reached its maximum 3 hours and 25 min after the start of irradiation, and then started to decrease gradually due to the dominance of particle wall losses. Aerosol mass concentrations can be corrected for wall losses based on the observed decay of the particle mass (volume from SMPS measurements) concentration, when particle formation has ceased to take place. This is particularly important for particle and product yield studies, where the quantity of aerosol produced in a clean environment is estimated from the final aerosol volume. However, this is not the focus of this study and therefore, data were not corrected for wall losses. The delay between particle detection by the CPC and the AMS is due to the difference in particle size detection limit of both

instruments (3 nm for the CPC and about 40 nm for the AMS). As a result the AMS could only provide information on the particle growth and not nucleation. Gas phase measurements showed that ozone levels were below 1 ppb at the beginning of each experiment and increased slowly as NO was converted to NO_2, and then increased rapidly and peaked at about 300 ppb as the NO mixing ratio decreased to values below 1 ppb. The gas phase data are discussed in more detail in separate publications [*Kalberer et al., 2004; Paulsen et al., 2004*].

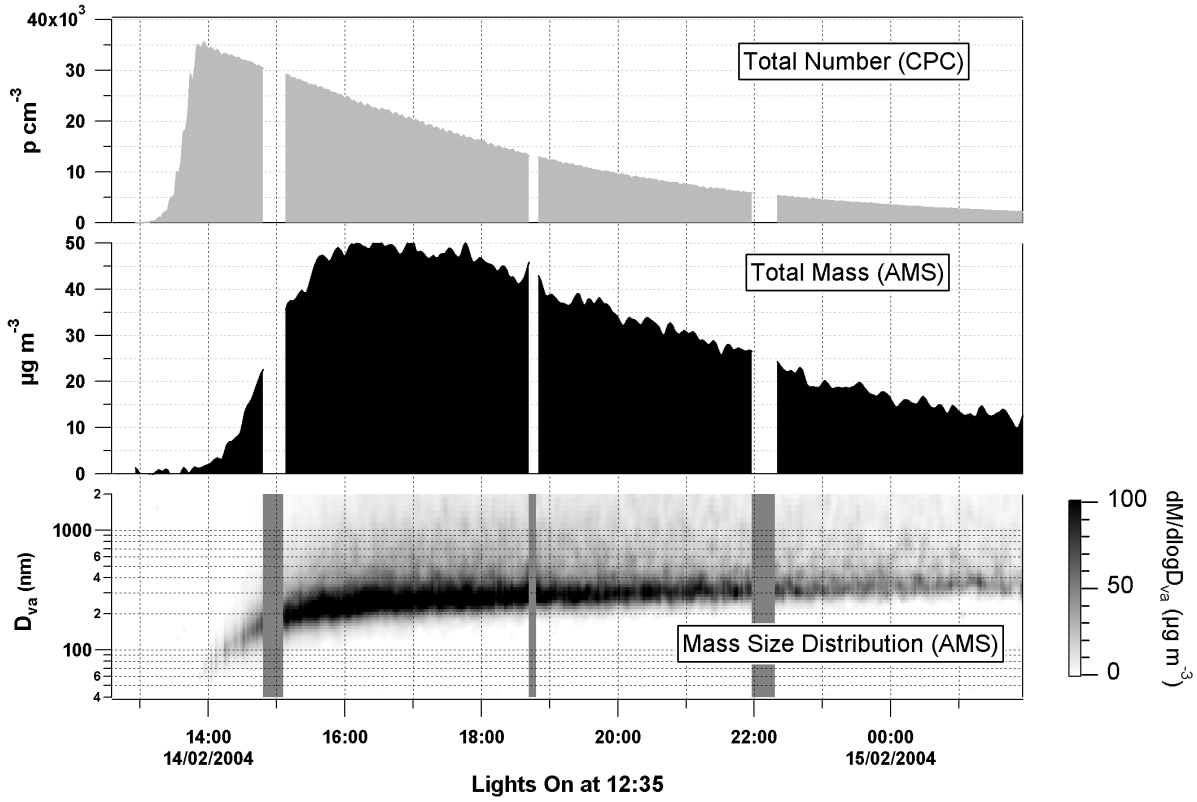

Figure 6.1: Time profile of the evolution of particles during a 'high' concentration 1,3,5-TMB experiment (experiment number 3, Table 1), showing the total particle number concentration (p/cm^3) counted by the CPC in the top panel, the total mass loading (µg/m^3) measured by the AMS in the middle panel and particle mass size distribution measured as a function of its vacuum aerodynamic diameter in the bottom panel. Note that data is not corrected for wall losses. The tail off in mass loading at the high sizes above the main mode is not due to large particles, but results from high particle loads slowing the normally near instantaneous vaporisation of particles.

6.4 Chemical signatures

One of the main objectives of this study is to investigate the change of the chemical signature of the photooxidation products of both precursors as a function of irradiation time. This will be first discussed for the products of each precursor followed by a comparison of their signatures at similar time intervals. The two 'high' concentration experiments for each precursor (experiments 2 and 3 for 1,3,5-TMB and 4 and 6 for α-pinene, Table 6.1) resulted in highly reproducible mass spectra and SOA concentrations. The chemical signatures of the 'high' and 'low' concentration experiments of α-pinene (experiments 4 and 6, Table 6.1) were similar. On the other hand, low signal to noise levels in the 'low' concentration 1,3,5-TMB (experiment 1, Table 6.1) did not allow a useful comparison with the 'high' concentration 1,3,5-TMB experiments. As a result, it is important to note that all spectra discussed in this chapter for the photooxidation products of 1,3,5-TMB and α-pinene are from the 'high' concentration experiments 3 and 4, respectively, in Table 6.1. It is also worth noting that the reported chemical signatures are for the growing (> 40 nm), not nucleating (~ 3 nm), particles in each case. Figure 6.2 shows mass spectra of the photooxidation products of 1,3,5-TMB (panels A – C) and α-pinene (panels D – F) averaged for one hour each after 3, 5 and 8 hours of irradiation. All spectra are normalised to the sum total of all mass fragments, providing a quantitative fractional contribution of each mass fragment to the total measured mass.

6.4.1 Discussion of the chemical signatures of the photooxidation products of 1,3,5-TMB and α-pinene

The mass spectra of the photooxidation products of both 1,3,5-TMB and α-pinene are characterised by a very intense mass fragment at *m/z* 43, contributing about 18 and 13%, respectively, to the total produced mass in each case. As discussed in chapter 5, this fragment arises, typically, from either saturated hydrocarbons in the form of ($C_3H_7^+$), or from oxidised, carbonyl-containing compounds (e.g. aldehydes and ketones) in the form of (CH_3CO^+), which is more likely to be the case in this study. Mass fragment 44 corresponds to the CO_2^+ fragment and laboratory experiments described in chapter 4 have shown that it arises, along with at least a similar amount of mass fragment 18 (H_2O^+), from decarboxylation of oxo- and di-carboxylic acids, as well as

highly oxidised compounds such as fulvic acid (see chapter 5, section 5.6.3), which represents an example of humic-like substances. As previously discussed, the mass fragment 18 also contains large contributions from gas phase water, sulphate and other species. To retrieve the total organic mass loading, the contribution of water resulting from decarboxylation at *m/z* 18 is set equal to *m/z* 44 based on laboratory results with pure compounds performed in argon, where the interferences to *m/z* 18 are eliminated [*P. Silva, Utah State University, Personal Communication*]. As a result, there is no independent information about the mass spectral signature of the observed organic in these experiments at *m/z* 18. The two fragments together contribute up to at least 12 and 16% to the total mass that is produced from the aerosol products of 1,3,5-TMB and α-pinene, respectively.

Mass fragments 15, 27 and 29 are signatures of the short carbon chains CH_3^+, $C_2H_3^+$ and $C_2H_5^+$, respectively, which most likely form part of the carbon structure of the oxidised compounds discussed above. In addition *m/z* 29 may also have a contribution from the HCO^+ ion resulting from carbonyl-containing compounds. They contribute a total of about 14 and 13% to the total produced mass from the products of 1,3,5-TMB and α-pinene, respectively. In total, these 6 mass fragments account for about 44 and 42% of the total produced mass from 1,3,5-TMB and α-pinene products, respectively, indicating that the particles produced from the photooxidation of both precursors are highly oxidised in nature and are dominated by carbonyl and oxidised carboxylic acid functional groups. This is in agreement with previous reaction chamber studies, where highly oxidised chemical classes including di-, keto-, and hydroxy-keto- carboxylic acids in addition to ketones, keto-aldehydes, hydroxy-keto-aldehydes and hydroxy-ketones have been reported, in different concentrations and distribution patterns, as photooxidation products of aromatic and monoterpene compounds [*Forstner et al., 1997; Glasius et al., 2000; Jang and Kamens, 2001; Larsen et al., 2001; Jaoui and Kamens, 2003; Kleindienst et al., 2004*].

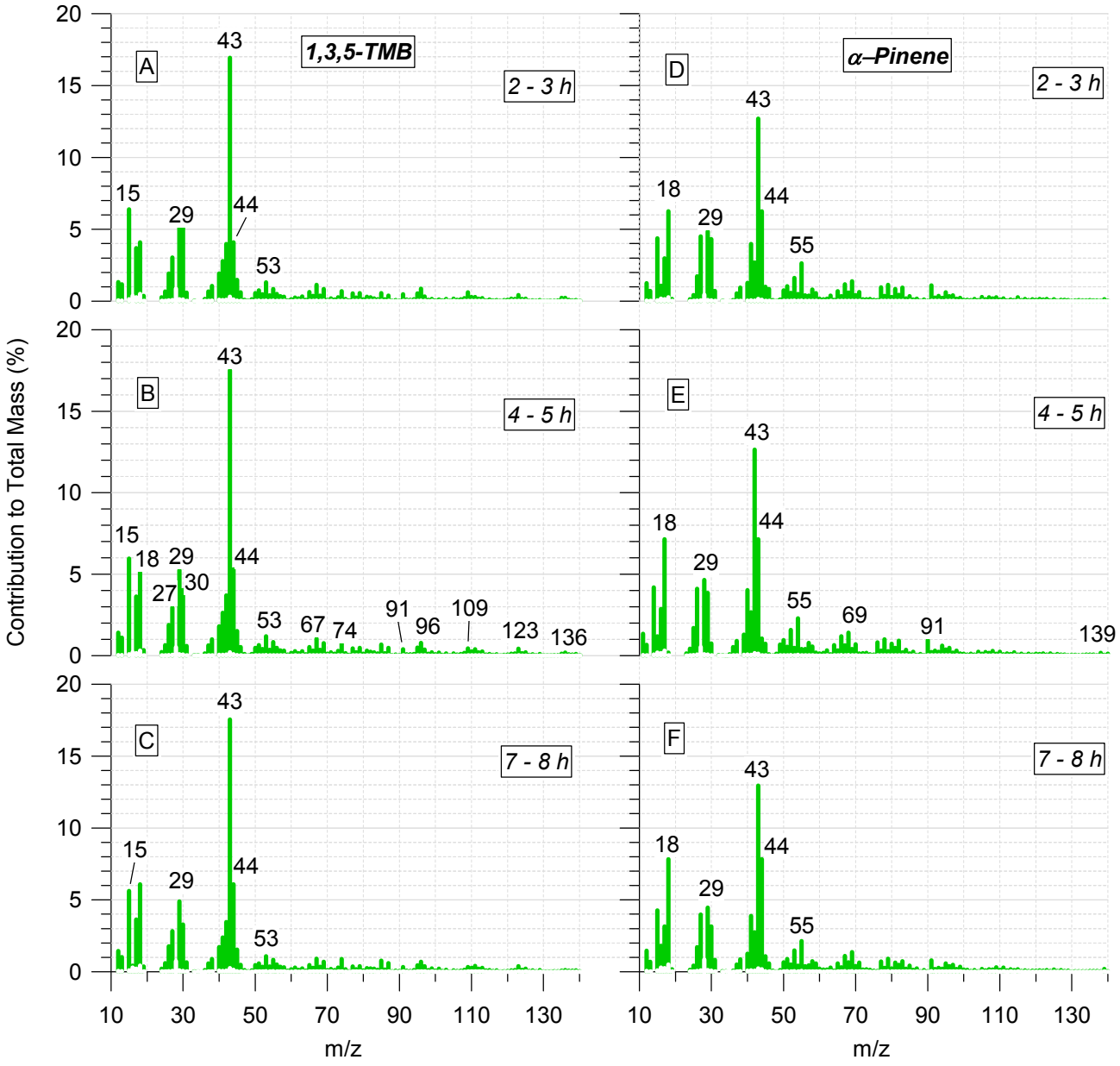

Figure 6.2: Mass spectra of the photooxidation products of 1,3,5-TMB and α-pinene averaged for one hour each after 3, 5 and 8 hours of irradiation. All spectra are normalised to the sum total of all mass fragments, providing a quantitative fractional contribution of each mass fragment to the total measured mass. The white bars at the bottom of individual mass fragments are the associated errors.

A large number of low-intensity fragments account for the rest of the produced mass. These fragments typically contribute less than 3% each to the total produced mass from each precursor, but are clearly observable above the background. Figure 6.3 displays the mass spectra shown in panels A and D in Figure 6.2 on a logarithmic scale in order to

better illustrate the distribution patterns of the low-intensity mass fragments in each case. The relatively low contributions of these fragments to total mass do not, necessarily, indicate that they are insignificant in terms of their chemical signature. It is likely that many of their parent molecules are thermally unstable at the vaporisation temperature of the AMS (550 ^{o}C), and they are readily converted into smaller forms before being ionised. This may, as a result, enhance the intensity of the small fragments. However, this does not rule out a second possibility, whereby the photooxidation products yield these low mass fragments directly as major ionisation products.

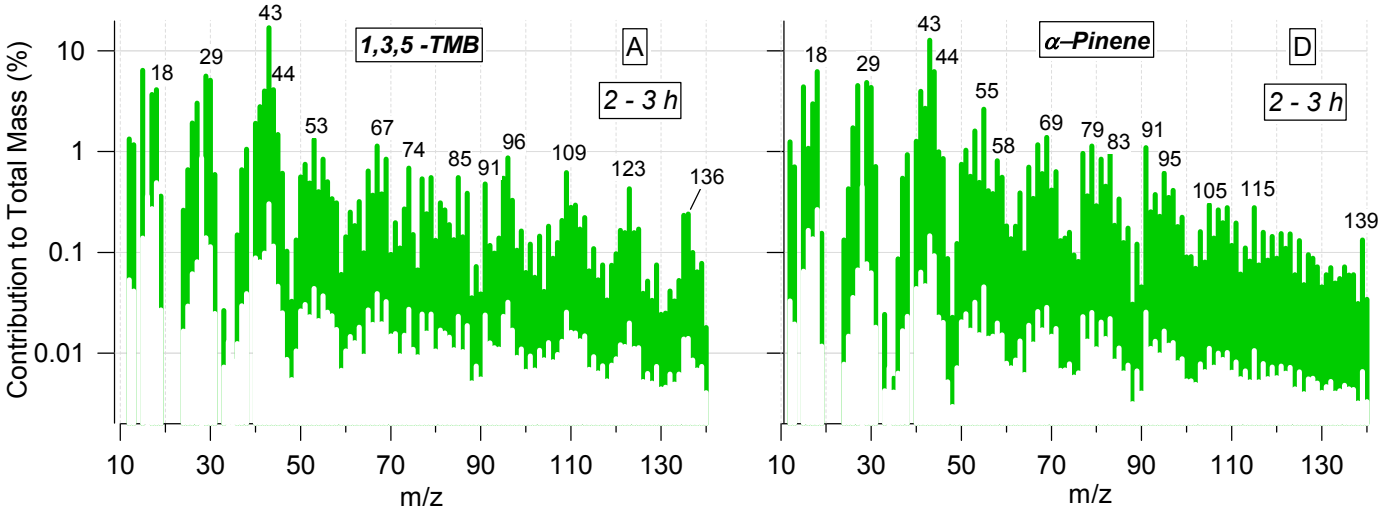

Figure 6.3: A logarithmic scale presentation of the mass spectra shown in panels A and D in Figure 6.2 in order to better illustrate the distribution patterns of the low-intensity mass fragments produced from the photooxidation of 1,3,5-TMB and α-pinene. The white bars at the bottom of individual mass fragments are the associated errors.

6.4.2 Mass spectral signatures as a function of irradiation time

The time resolved mass spectra of the 1,3,5-TMB products (panels A – C in Figure 6.2) appear to have highly similar fragmentation patterns, implying that the chemical signature of the products does not markedly change overall with irradiation time. This is also true for mass spectra of the α-pinene products (panels D – F in Figure 6.2). This finding was further examined through a detailed inspection of hourly averaged mass spectra throughout the duration of each experiment (not shown in Figure 6.2). In order to quantify these similarities, the hourly averaged mass spectra from Figure 6.2 measured at 5 and 8 hours were compared to those measured at 3 hours of irradiation

time for each precursor. Pearson's *r* values of 0.99 and 0.98 for the 1,3,5-TMB comparisons and 1.00 and 0.99 for the α-pinene case were found and are shown in Figure 6.4, confirming that the chemical signature of the photooxidation products of each precursor after 5 and 8 hours of irradiation time does not appear to change from that after only 3 hours of irradiation.

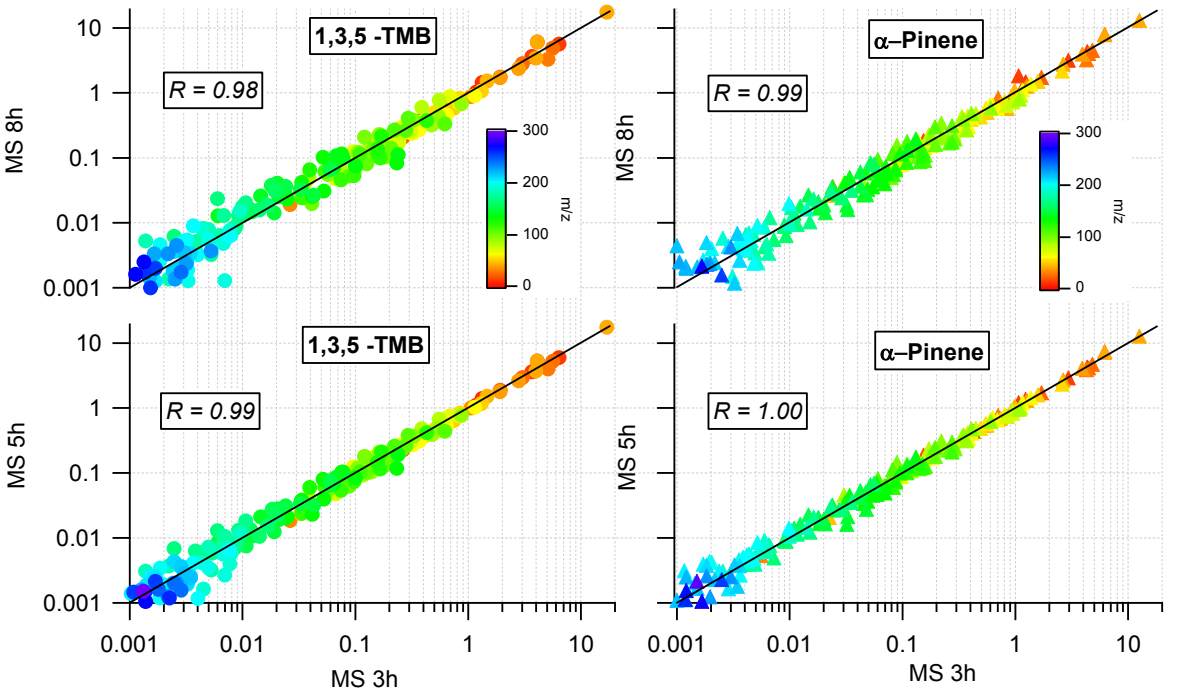

Figure 6.4: Comparison of the fragmentation patterns of the photooxidation products of 1,3,5-TMB after 5 and 8 hours with that after 3 hours of irradiation. The plotted data are the fractional contributions to total mass of each mass fragment as shown in Figure 6.2. The colour scale is a function of m/z number and the black line is the slope of unit gradient. An identical comparison of the α-pinene data is also shown.

This indicates that once particles are formed, it is unlikely that long periods of irradiation lead to a significant change in the particle chemical signature measured by the AMS. However, evidence of polymerisation has recently been reported under the same conditions, showing an increase in the particle non-volatile fraction as well as high molecular weight mass fragments (m/z > 400) as a function of irradiation time [*Kalberer et al., 2004*]. On the other hand, the ratio of the volume concentration (measured by the SMPS) and the mass concentration (measured by the AMS) remained constant over the time of the experiment, even though the AMS only reports mass

fragments up to *m/z* 300. Therefore it is likely that the large molecules break into fragments mainly below *m/z* 200 in the AMS upon volatilisation and ionisation.

Although the overall fragmentation patterns of the photooxidation products from both precursors did not change substantially over the duration of each experiment (i.e. the order of magnitude of the fractional contribution to the total mass by individual mass fragments after 5 and 8 hours remained as it was after 3 hours of irradiation), the contribution of some individual mass fragments to total mass appeared to be influenced by the irradiation time. The effect of irradiation time on the fractional contribution of individual mass fragments to the total mass after 5 and 8 hours relative to that after 3 hours of irradiation is shown in Figure 6.5 for both precursors, and was calculated for the mass spectra shown in Figure 6.2 by comparing the percentage change, D, of each mass fragment at 5 and 8 hours compared to that observed at 3 hours using the following expression:

$$D(\%) = \left(\frac{MS_{ih} - MS_{3h}}{MS_{3h}} \right) \cdot 100 \qquad (6.1)$$

where MS_{ih} refers to the mass spectra after 5 and 8 hours and MS_{3h} to the mass spectra after 3 hours of irradiation in Figure 6.2.

Figure 6.5 shows that the fractional contribution of some mass fragments to total mass increases with irradiation time. For example, the fractional contribution of *m/z* 44 (CO_2^+ from highly oxidised acidic compounds), appears to increase after 8 hours of irradiation by about 50% and 25% relative to its contribution after 3 hours of irradiation in the cases of 1,3,5-TMB and α-pinene, respectively. These temporal changes are similar to the increases observed in the low volatile fraction of the aerosol measured by the VTDMA in these experiments and those reported by *Kalberer et al.*, [*2004*]. Interestingly, the fractional contributions of larger mass fragments, such as *m/z* 127, 140 and 155 in the 1,3,5-TMB case and *m/z* 100 and 156 in the α-pinene case, appear to increase after 8 hours of irradiation by as much as 100% and 75%, respectively, indicating that the significance of larger mass fragments increases with irradiation time.

Although the actual contributions of these mass fragments to total mass are very low, this could be indirect evidence for the formation of large molecules in both systems. On the other hand, Figure 6.5 shows that the fractional contributions of other mass fragments to total mass appear to decrease with irradiation time. It is possible that these changes are due to oxidation of the molecules in the aerosol over time.

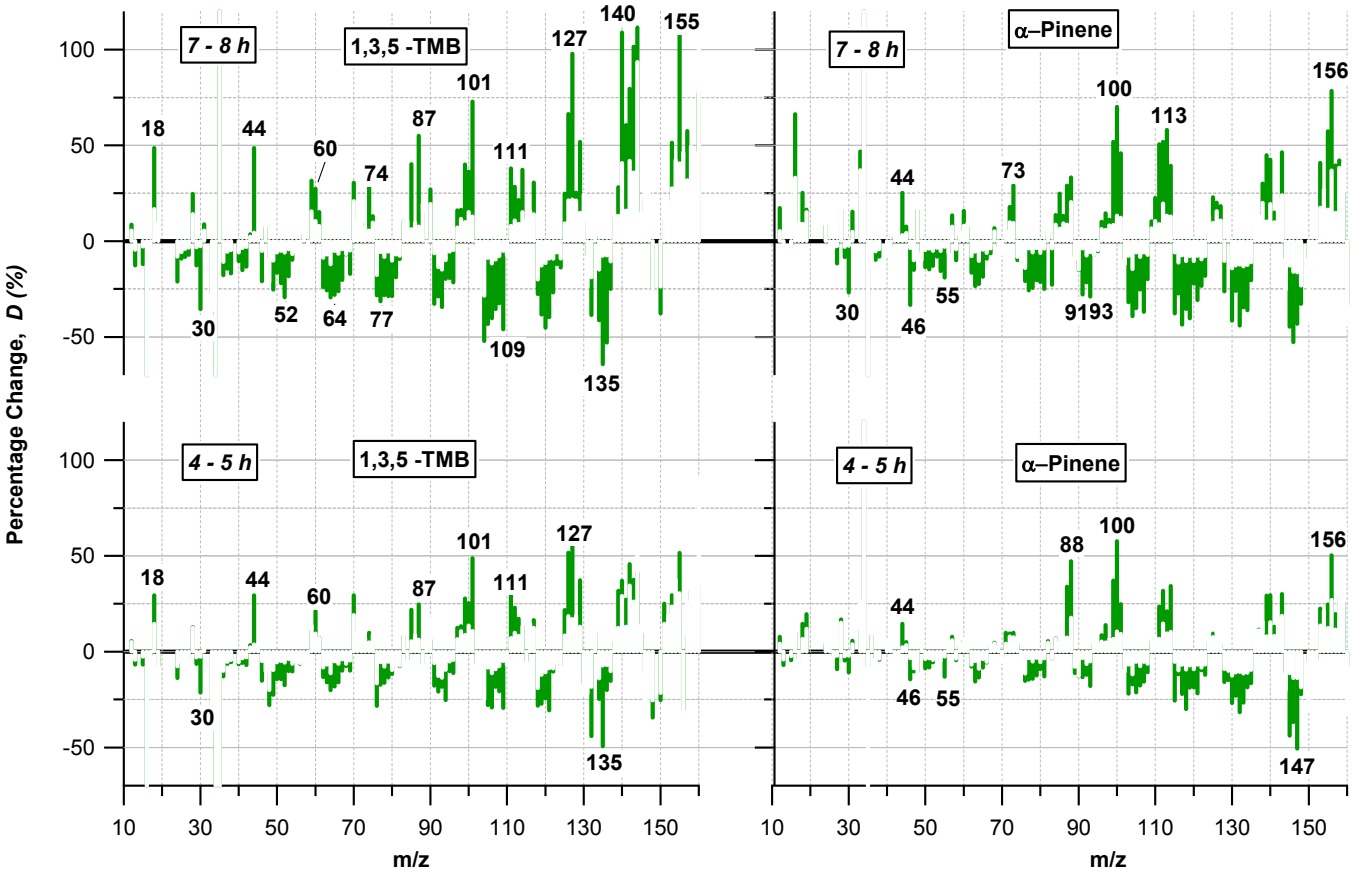

Figure 6.5: The percentage change (D %) in the fractional contribution to total mass of individual mass fragments at 5 and 8 hours compared to that observed at 3 hours of irradiation for the photooxidation products of 1,3,5-TMB and α-pinene calculated using equation6.1. The white bars on the individual mass fragments are errors propagated through equation 6.1.

6.4.3 Comparison of the chemical signatures of the photooxidation products of 1,3,5-TMB and α-pinene

Another objective of this study is to investigate how the mass spectral signature of the photooxidation products changes between typical anthropogenic (1,3,5-TMB) and biogenic (α-pinene) precursors. The mass spectra in Figure 6.2 illustrate that the chemical signature of the products from both precursors, after equal periods of

irradiation, are broadly similar. Both spectra are dominated by mass fragment 43 and, to a lesser extent, mass fragment 44 representing highly oxidised classes of compounds containing carbonyl and carboxylic acid functional groups. One possible reason for the domination of mass fragment 43 in mass spectra is the use of propene in all experiments as a source of radicals. The photooxidation of propene is known to produce compounds like acetaldehyde and acetic acid, which produce mass fragment 43 as one of their main fragments upon ionisation by a 70 eV EI source [*McLafferty and Turecek, 1993*]. However, this is likely to account for part, but not all of the contribution of mass fragment 43 to total mass.

Because of the extensive fragmentation caused by electron impact ionisation and the similarity in mass spectra of compounds in the same chemical classes, most mass fragments appear to be present in the mass spectra of the SOA produced from both precursors. A detailed study of the mass spectra in Figures 6.2 and 6.3 shows, however, that subtle differences do exist between the two chemical signatures. For example, *m/z* 43 contributes about 17% to the total mass produced from 1,3,5-TMB, while it contributes 13% in the α-pinene case. On the other hand, mass fragments in the 50 to 100 *m/z* range appear to be more pronounced in the α-pinene case. Another consistent difference is in the 53/55 and 67/69 mass fragment ratios, where the smaller mass fragment appears to be always higher in the 1,3,5-TMB spectra, while the opposite is true in the α-pinene case. Furthermore, mass fragments 74, 96, 135, 136 and the ion series 95, 109, 123 appear to be more strongly associated with 1,3,5-TMB, and mass fragments 58, 83, 115, 139, 141, 167 and 199 with α-pinene.

More differences in the chemical composition of the SOA formed from the two precursors can be drawn from Figure 6.5. It shows that the mass fragments that have increasing fractional contribution to total mass as a function of irradiation time are distinctly different for the two precursors. These mass fragments include 59, 74, 87, 101, 127, 140 and 155 in the case of 1,3,5-TMB and 73, 100, 113 and 156 in the α-pinene case. Although it is not possible to exclusively relate the individual mass fragments to specific chemical compounds, the above observations indicate that the SOA produced from each precursor has broadly similar chemical functionality given by

the high abundance of *m/z* 43 and 44. However, significant differences occur in the minor fragments for the SOA in the two reaction systems, indicating that the precise molecular composition differs.

6.5 Formation of nitrogenated organic compounds

Mass fragments 30 and 46 observed with the AMS during atmospheric sampling have been mostly interpreted as NO^+ and NO_2^+ from inorganic nitrate compounds [*Allan et al., 2003a; Jimenez et al., 2003b; Boudries et al., 2004*]. In this study, both fragments were observed in the mass spectra of the photooxidation products of both precursors (Figure 6.2). The temporal behaviour of both fragments was found to be very similar within each of the experiments. This similarity is quantified in Figure 6.6, where concentrations of mass fragments 30 and 46 are correlated for each precursor. Both correlations have high Pearson's *r* values of 0.98 and 0.92 for 1,3,5-TMB and α-pinene, respectively. However, their temporal behaviour is significantly different to other major fragments observed, and appeared to be controlled by the temporal variability of NO_x. This indicates that, in each case, both fragments are likely to have the same chemical source.

Organic nitrates and nitro-compounds are possible candidates. Laboratory studies (see chapter 4, section 4.5) showed that for inorganic nitrate salts, the ratio of mass fragments 30 to 46 varies with the type of cation in each salt. For example, the 30/46 ratio is 2 to 3 for ammonium nitrate, 11 for magnesium nitrate and 29 for sodium nitrate. In this study, the 30/46 ratio is 8 for the products of 1,3,5-TMB and 5 for the α-pinene case. The ratio was constant over the duration of both experiments. The different values of the 30/46 ratios may imply that different nitrogenated compounds are formed from each precursor. The formation of nitro organic compounds has already been reported in a number of chamber studies.

Forstner et al., [*1997*] presented a detailed mechanism leading to the formation of nitro aromatic compounds from the photooxidation of toluene in the presence of NO_x and propene. Pathways for production of nitrophenolic compounds from an ethylbenzene-OH adduct were also discussed. In a similar recent study, *Kleindienst et al.*, [*2004*]

suggested that NO_2 addition to aromatic rings becomes more significant at elevated concentrations of NO_2, which is usually the case in environmental chamber studies. It was explained that the NO_2 addition stabilises the ring intermediate leading to the formation of nitro and di-nitro aromatic compounds. In a third study of the same system, the contribution of alkyl nitrates ($RONO_2$) or peroxyacyl nitrates ($RC(O)OONO_2$) to the secondary organic aerosol formation was positively verified using FTIR spectroscopy [*Jang and Kamens, 2001*]. In addition, many studies have examined and reported the formation of nitrate compounds from the oxidation of α-pinene and other terpenes [*Noziere and Barnes, 1998; Kamens and Jaoui, 2001*]. Mono- and di-alkyl nitrates, peroxyacetylnitrate (PAN) and PAN-related compounds were among the reported compounds [*Jaoui and Kamens, 2003*].

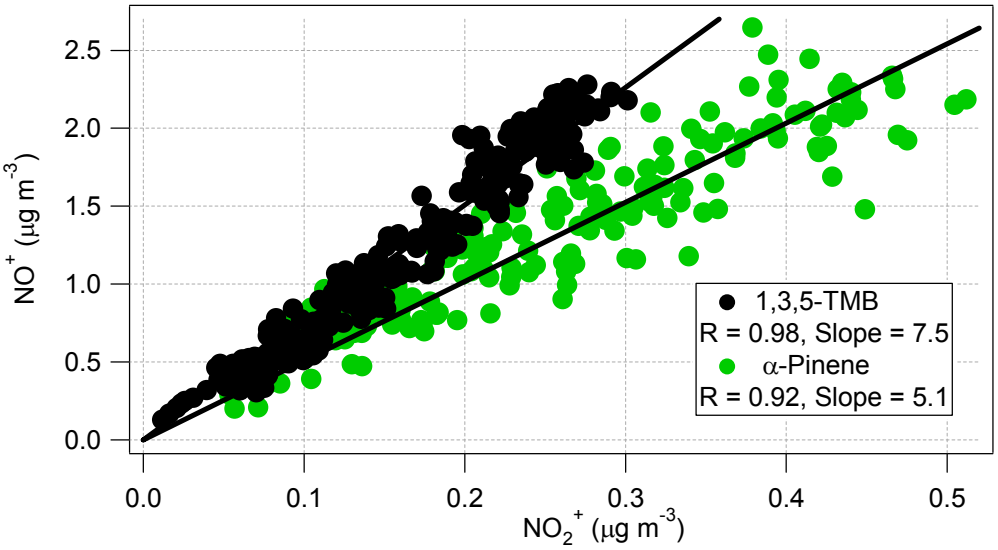

Figure 6.6: Correlation of the mass concentrations of mass fragments 30 (NO^+) and 46 (NO_2^+) produced from the photooxidation of 1,3,5-TMB and α-pinene.

The time-resolved mass spectra in Figure 6.2, as well as the time-varying relative fractional contributions of individual mass fragments to total mass in Figure 6.5 show that the contributions of the mass fragments 30 and 46 to total mass decrease with time for both precursors. The contribution of the sum of NO^+ and NO_2^+ to the total particulate mass spectrum starts as high as 7% and decreases to about 3% after about 8 hours of irradiation. This is likely to be explained by the consumption of the gas phase NO_x after only 3 and 5 hours of the start of 1,3,5-TMB and α-pinene experiments, respectively.

6.6 Formation of model polymers in the absence of oxidation

About 30 small carbonyls and acids have been recently measured in the gas and particle phase products of an identical 1,3,5-TMB photooxidation experiment to the one discussed in this study [*Kalberer et al., 2004*]. GC-MS and ion chromatography (IC) were used to identify the oxidation products [*Fisseha et al., 2004*]. Methylglyoxal, a C_3-dicarbonyl, was found to be one of the most abundant gas-phase photooxidation products of 1,3,5-TMB. Recent studies have suggested that additional partitioning of carbonyls to particle phase may occur via chemical transformation of the carbonyls to low volatility products [*Tobias and Ziemann, 2000; Jang et al., 2003*]. The hydration of the carbonyl followed by acid-catalysed polymerisation or acetal/hemiacetal formation in the presence of alcohol have been reported as a potential mechanism for this transformation [*Jang et al., 2003*].

An aqueous solution of glyoxal is composed of a mixture of hydrated monomers, dimers and trimers forming acetals [*Kalberer et al., 2004 and reference therein*]. Laser Desorption Ionisation Mass spectrometry (LDI-MS) measurements of methylglyoxal showed oligomers up to the nonamer with m/z = 723. An LDI mass spectrum of an equal-mass aqueous solution of methylglyoxal, formaldehyde, 3,5-dimethylbenzaldehyde and pyruvic acid (all known oxidation products of 1,3,5-TMB) showed an oligomer pattern similar to that produced from the photooxidation products of 1,3,5-TMB in the range $400 < m/z < 900$. On this basis, *Kalberer et al.,* [*2004*] proposed a nonradical-induced acetal polymerisation with methylglyoxal as the main monomer unit, with the possibility that other carbonyls and carbonyl-containing acids may also be incorporated into the polymer. The polymer fraction was quantified using a volatility tandem differential analyser (VTDMA), which measures the size reduction of the aerosol due to evaporation in a heater that has tube wall temperatures of 100, 150, and 200 ^{o}C [*Rader and McMurry, 1986*]. Measurements showed that the particle volume fraction remaining at 100 ^{o}C gradually increased from about 30% to 85% over 27 hours of irradiation. This increase in nonvolatile particle fraction was mostly attributed to polymer formation. Similar measurement trends were reported at 150 ^{o}C and 200 ^{o}C. Moreover, the lack of significant increase in the hygroscopic growth of the particles after the first 8 hours of irradiation (growth factor around 1.10 at 85% RH) was

interpreted as an additional indication that polymers and not more hygroscopic, highly oxidised individual reaction products (such as multifunctional acids) were mainly responsible for the increasing low volatility fraction of the particles. The VTDMA results of 1,3,5-TMB photooxidation products were reproduced during the study presented in this paper and similar trends were also measured for the α-pinene photooxidation products.

In order to further investigate the role of the polymerisation and photooxidation processes in these experiments, organic particles were generated using solutions of methanol and methylglyoxal, particle-free pure air, and a collison atomiser [*May, 1973*]. The particles were delivered into a 200 litre, opaque, carbon-impregnated, polyethylene plastic bag, in the absence of NO_x, propene and irradiation. The AMS and the VTDMA were used to simultaneously measure the methylglyoxal particles over approximately 2 hours. The VTDMA results using a heater wall temperature of 100 ^oC showed that the remaining non-volatile particle volume fraction increased from 38% to 46% over 1.5 hrs, giving a rate of 4.7% hr^{-1} (4.3% hr^{-1} for an aqueous methylglyoxal solution, rates determined from a linear least-squares regression). A similar analysis of the linear portion of reaction chamber data (first 8 hrs, data from *Kalberer et al., 2004*) for high and low concentration 1,3,5-TMB cases produced rates of 3.7% hr^{-1} and 3.1% hr^{-1}, respectively. These similar rates demonstrate that photochemistry is not required for methylglyoxal to polymerise. A similar VTDMA result revealed a slower polymerisation rate of 2.6% hr^{-1} when the same experiment was repeated using the four-compound mixture of methylglyoxal, formaldehyde, 3,5-dimethylbenzaldehyde and pyruvic acid reported in *Kalberer et al.,* [*2004*].

Figure 6.7 shows the averaged mass spectra of the methylglyoxal (bottom panel) and the mixture compounds (middle panel) polymerisation products measured by the AMS. Although the molecular weight of methylglyoxal is 72, its mass spectrum shows mass fragments larger than *m/z* 127. This observation supports findings of other studies regarding the presence of dimers and trimers in glyoxal solutions [*Kalberer et al., 2004 and references therein*]. A detailed investigation of the mass spectra of methylglyoxal and the mixture at high time resolution showed no significant change in the chemical

signature of any of them with time. This is likely because the polymer shows the same fragmentation pattern in the AMS as the monomer molecules. A comparison of the mass spectral signatures of the methylglyoxal and mixture polymerisation products in Figure 6.7 to that of 1,3,5-TMB photooxidation products in the top panel indicates some differences, particularly in the low intensity mass fragments above about *m/z* 50. The compounds introduced into the bag are those proposed by *Kalberer et al.*, [*2004*] as possible candidates for 1,3,5-TMB SOA formation. Whilst they do indeed lead to the formation of organic aerosol, the AMS fragmentation pattern observed are distinctly different from those measured from 1,3,5-TMB oxidation in the chamber. This supports the hypothesis of *Kalberer et al.*, [*2004*] of additional photooxidation products (e.g. other carbonyls) taking part in the polymerisation process.

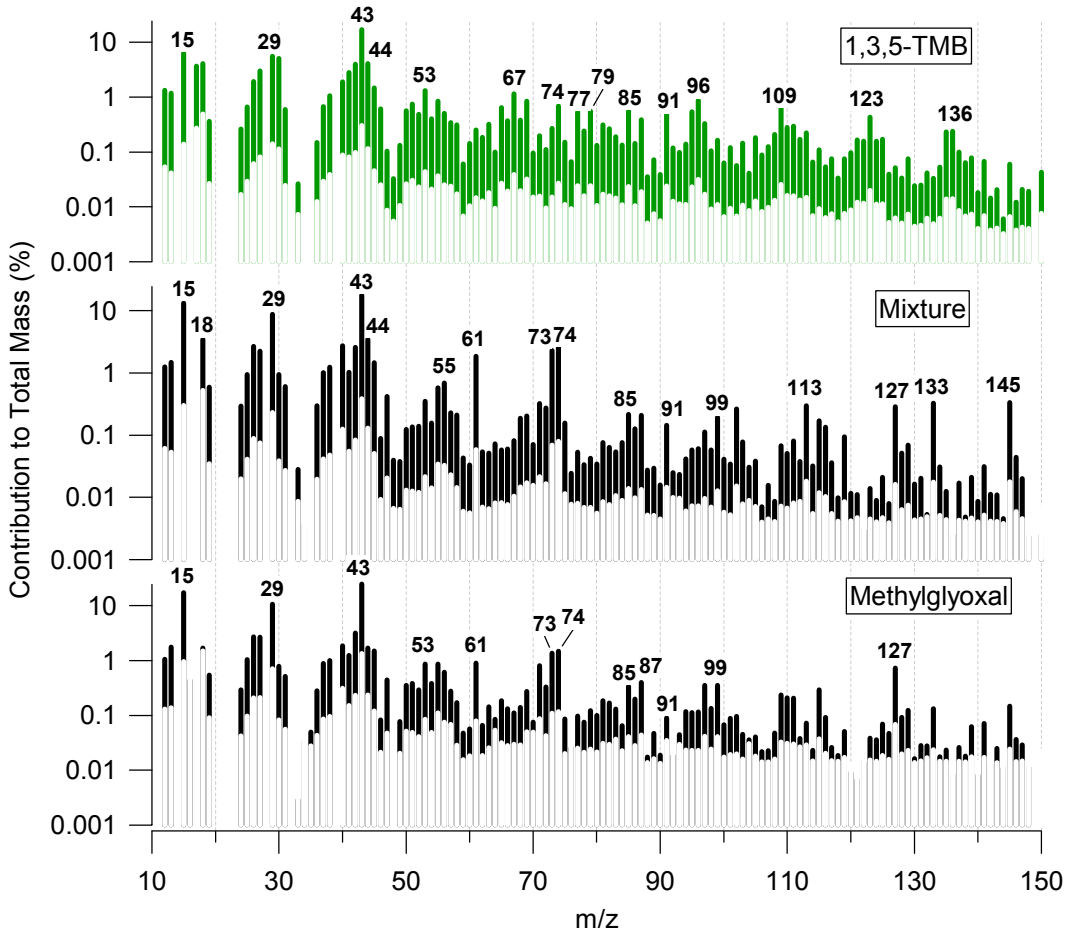

Figure 6.7: Mass spectral signatures of the polymers formed in the absence of oxidation by methylglyoxal, in the bottom panel, and the mixture of methylglyoxal, 3,5-dimethylbenzaldehyde, pyruvic acid and formaldehyde proposed by Kalberer et al., (2004), in the middle panel. The spectrum in the top panel is for the photooxidation products of 1,3,5-TMB as shown in panel A of Figured 6.3.

6.7 Atmospheric Implications

The lack of seed aerosol particles and the use of relatively high concentrations of precursors and NO_x mean that particles produced during this study are not expected to have chemical composition identical to ambient particles. However, the irradiation of 1,3,5-TMB and α-pinene in the presence of NO_x and propene may simulate the ambient photooxidation process of aromatic and biogenic precursors, respectively. In Figure 6.8, a compilation of mass spectra obtained from a number of AMS studies of the ambient atmosphere in various environments, along with the mass spectra of the photooxidation products of 1,3,5-TMB and α-pinene from this study (panels A and G, respectively) is presented. The aim is to evaluate how the mass spectral signatures of the photooxidation products of 1,3,5-TMB and α-pinene observed in this study compare to mass spectral signatures of the aerosol organic fraction measured in various environments affected to varying degrees by anthropogenic or biogenic precursors.

All spectra in Figure 6.8 are averaged over the duration of each experiment and are normalised to show the fractional contribution of each mass fragment to the total organic mass. The spectra in panels B and C are of the aerosol organic fraction at urban (Slocan Park) and rural (Langley) locations, respectively, in the Lower Fraser Valley, British Columbia, Canada and were measured as part of the Pacific 2001 experiment as discussed in chapter 5 [*Alfarra et al., 2004; Boudries et al., 2004*]. Panel D shows a mass spectrum of the particulate organic fraction measured at the remote high-alpine location Jungfraujoch (JFJ), Switzerland, during the second *Cloud-Aerosol Characterisation Experiment* (CLACE2) in 2002 (see chapter 7). The mass spectrum in panel E is from laboratory generated fulvic acid particles. Fulvic acid is a model compound for the water-soluble macromolecular group of "humic-like substances" (HULIS), which have recently been found to contribute 20 – 50% to the water-soluble fraction of organic aerosol at urban and rural sites, as well as fog samples in Europe [*Havers et al., 1998; Facchini et al., 1999a; Zappoli et al., 1999; Decesari et al., 2000; Krivacsy et al., 2000; Krivacsy et al., 2001b*]. The mass spectrum in panel F is from the particle growth period following a nucleation event at the forest research station at Hyytiälä in Finland during the second *Quantification of Aerosol Nucleation in the*

European Boundary Layer experiment (QUEST 2) in 2003 (Results from this experiment are not discussed in this thesis).

Inspection of the mass spectra in Figure 6.8 reveals that either or both of *m/z* 43 and 44 are the most dominant fragments in all cases; contributing up to 20% each to the total organic mass. As discussed before, *m/z* 43 arises from the ($C_3H_7^+$) fragment of saturated hydrocarbons in traffic-dominated environments and/or from the acetyl moiety of carbonyl-containing compounds (CH_3CO^+), which explains its significant contributions to the mass spectra measured in the traffic-dominated urban environment (panel B) and the biogenic compounds-dominated forest (panel F). On the other hand, mass fragment 44 was observed to be the AMS signature of highly oxidised compounds such as oxo- and di-carboxylic acids, and was also found dominant in a laboratory-generated mass spectrum of fulvic acid (Figure 6.8, panel E); a humic-like substance containing poly-carboxylic acid groups.

Carboxylic acids and humic-like substances have been widely reported in processed organic particles measured in various locations [*Havers et al., 1998; Facchini et al., 1999a; Zappoli et al., 1999; Decesari et al., 2000; Krivacsy et al., 2000; Krivacsy et al., 2001b*]. This appears to be in agreement with the mass spectra measured at the JFJ remote site (panel D) as well as the Canadian rural location (panel C); both dominated by processed aerosol particles. The urban organic mass spectrum in panel B is characterised by mass fragments (41, 43, 55, 57, 69, 71, …) representing the ion series $C_nH_{2n+1}^+$ and $C_nH_{2n-1}^+$ and separated by 14 mass units due to loss of CH_2. This spectrum is typical of hydrocarbons and has been associated with primary organic particles emitted from combustion sources (mainly traffic-related) in various urban locations as discussed in chapter 5 and reported in the literature [*Allan et al., 2003a; Alfarra et al., 2004; Canagaratna et al., 2004*].

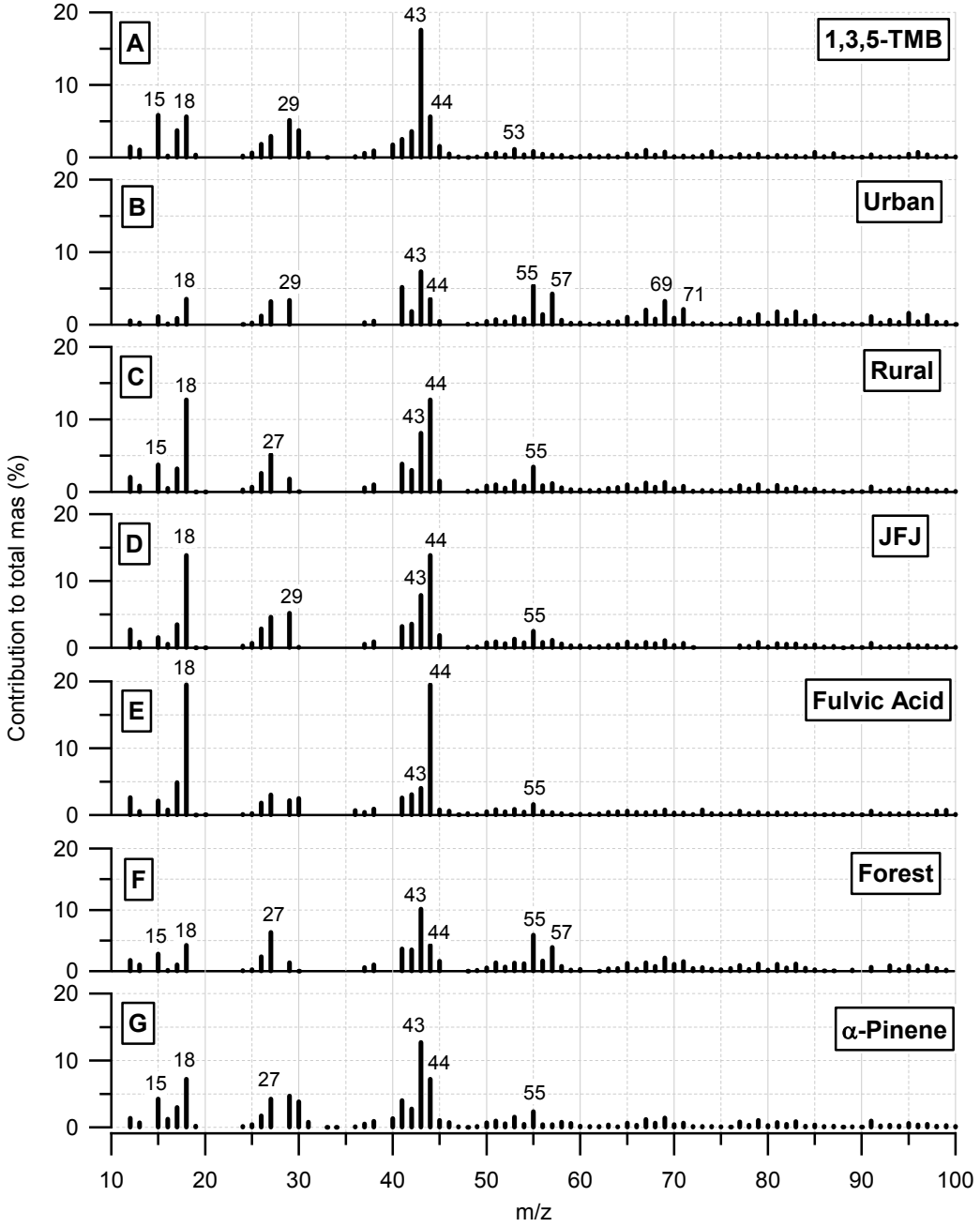

Figure 6.8: A compilation of AMS mass spectral signatures of SOA produced from 1,3,5-TMB and α-pinene from this study (panels A and G), laboratory generated fulvic acid particles (panel E) and organic particulate measured in the ambient atmosphere in urban (panel B) and rural (panel C) locations in British Columbia, Canada, the Jungfraujoch (JFJ) remote high-alpine location, Switzerland and a forest in Finland (panel F).

The emission of those primary organic particles prevents a meaningful comparison with the mass spectral signature of the photooxidation products of 1,3,5-TMB (panel A) as an anthropogenic precursor. While mass fragment 43 is expected to have contributions from both primary hydrocarbons as well as carbonyl-containing compounds produced in photooxidation processes in the former case, it can only arise as a result of the photooxidation process of 1,3,5-TMB in the latter. This may explain the more significant contributions of mass fragments larger than *m/z* 50 and the lower fractional contribution of mass fragment 43 in the urban spectrum compared to the 1,3,5-TMB spectrum. On the other hand, the photooxidation products of α-pinene appear to have a mass spectral signature (panel G) more similar to that of the particle growth following a nucleation event measured in a location dominated by biogenic emissions (panel F). In addition, the mass spectral signature of the α-pinene photooxidation products compares well to those of organic particulate at the rural and the remote alpine locations (panels C and D, respectively), with the exception that *m/z* 44 is more pronounced relative to *m/z* 43 at those two locations. This may be an indication that the organic particulate measured at the rural and high-alpine sites were more aged relative to SOA produced from the photooxidation of α-pinene. Moreover, the intensity of *m/z* 43 in the chamber experiments may have also been enhanced by contribution from propene oxidation products as discussed in section 4.3.

To quantify these comparisons, the mass spectral signatures of the organic particulates measured at the locations above were scatter plotted against the mass spectra of fulvic acid, 1,3,5-TMB SOA products and α-pinene SOA products and the resulting Pearson's *r* values are summarised in Table 6.2. Results indicate that the mass spectral signature of the humic-like substance (fulvic acid) is significantly more similar to the organic signatures at the rural and remote alpine sites than to those of the urban and freshly nucleated forest particles. This may explain, in part, the dominance of *m/z* 44 at the former locations. The results also reveal that the photooxidation products of α-pinene explain more of the chemical signature of organic particulate at those locations compared to 1,3,5-TMB. This could be due to the reported higher aerosol formation potential of biogenic compounds compared those from anthropogenic sources [*Odum et al., 1996; Griffin et al., 1999*] and to the fact they are emitted in much more significant

amounts into the atmosphere. The total annual global emission of biogenic compounds has been estimated between 825 Tg C yr^{-1} [*Fehsenfeld et al., 1992; Guenther et al., 1995*], whereas anthropogenic compounds have been estimated to account for less than 100 Tg C yr^{-1} [*Hough and Johnson, 1991; Muller, 1992*].

	1,3,5-TMB	α-Pinene	Fulvic Acid
Urban	0.71	0.80	0.50
Rural	0.75	0.87	0.93
JFJ	0.73	0.85	0.94
Forest	0.80	0.86	0.54

Table 6.2: Pearson's R values resulting from the correlations of the mass Spectra in Figure 8

6.8 Summary

Recent studies have reported that polymers and oligomers compose significant fractions of SOA formed from the photooxidation of aromatic and biogenic compounds. The AMS was utilised in this study to provide on-line measurements of the mass spectral signatures and mass size distributions of the oxidation products resulting from irradiating 1,3,5-trimethylbenzene and α-pinene, separately, in the presence of nitrogen oxide, nitrogen dioxide and propene in a reaction chamber. Mass spectral results indicate that the SOA produced from each precursor has broadly similar chemical functionality of highly oxidised nature given by the abundance of *m/z* 43 and 44. However, significant differences occur in the minor mass fragments for the SOA in the two reaction systems, indicating that they have different molecular composition. Nitrogenated organic compounds have been observed in the photooxidation products of both precursors, and their formation appeared to be controlled by the temporal variability of NO_x. However, different types of nitrogenated compounds may have been formed in each system. Although the overall fragmentation patterns of the photooxidation products in both systems did not change substantially over the duration of each experiment, the contribution of some individual mass fragments (such as *m/z 44*) to total mass appeared to be influenced by the irradiation time. Investigation of the influence of the polymerisation and photooxidation processes on the 1,3,5-TMB reaction products found that while polymerisation of methylglyoxal as well as the four-compound mixture proposed by *Kalberer et al.,* [*2004*] occurs in the absence of

photooxidation, the observed mass spectral signatures appear to be different to that of SOA produced from 1,3,5-TMB in the chamber. This supports the hypothesis of *Kalberer et al.*, [*2004*] suggesting that additional photooxidation products (e.g. other carbonyls) to those proposed in the mixture may also participate in the polymerisation process. Finally, results suggest that the photooxidation of α-pinene explain more, compared to 1,3,5-TMB, of the chemical signature of organic particulate observed at various urban, rural and background locations.